Spatial Probability Characteristics of Waves Generated by Polar Lows in Nordic and Barents Seas

Maria Yurovskaya, Vladimir Kudryavtsev, Bertrand Chapron

remote sensing

MDPI

Article

Spatial Probability Characteristics of Waves Generated by Polar Lows in Nordic and Barents Seas

Maria Yurovskaya [1,2,*], Vladimir Kudryavtsev [1,2] and Bertrand Chapron [3]

[1] Marine Hydrophysical Institute, 299011 Sevastopol, Russia; kudr@rshu.ru
[2] Satellite Oceanography Laboratory, Russian State Hydrometeorological University, 195196 St. Petersburg, Russia
[3] Laboratoire d'Océanographie Physique et Spatiale (LOPS), Univ Brest, CNRS, IRD, Ifremer, 29280 Plouzané, France; bertrand.chapron@ifremer.fr
* Correspondence: m.yurovskaya@mhi-ras.ru

Abstract: Polar lows (PLs) are mesoscale, up to 1000 km, rather short lifetime (less than 15–30 h) cyclonic atmospheric systems formed in polar latitudes and associated with cold outbreak events. Strong winds, higher than 15 m/s, can then generate high surface waves which may pose danger to marine and coastal infrastructures. To investigate the probability of high waves generated by PLs in the Nordic and Barents Seas, analysis can be performed using available PL statistical distributions obtained from satellite passive microwave data, MODIS infrared imagery and ASCAT scatterometer data. Classical self-similar laws for wind waves development based on the extended duration concept are used to obtain first-guess estimates of significant wave height and the wavelength of waves generated by PL. All possible combinations of PL parameters (maximum wind speed, lifetime, diameter, translation velocity and direction of propagation) are considered to obtain the occurrence of waves exceeding specified levels, ranging from 2 to 15 m for significant wave height and from 100 to 500 m for wavelength. Particularly, PL-generated waves higher than 4 m occur up to 6 times a year, higher than 8 m occur up to 2–3 times a year, higher than 10 m occur up to once a year, the probability of 12 m waves is one event in several years and 15 m SWHs occur less than once in a decade. The area most affected by strong waves from PLs is the near shore zone around the Scandinavian peninsula, northward from the North Cape. The relative contribution of PLs in the formation of the waves field in the Nordic and Barents Seas is discussed.

Keywords: polar lows; wind waves generation; significant wave height; abnormally high waves; wave predictions

Citation: Yurovskaya, M.; Kudryavtsev, V.; Chapron, B. Spatial Probability Characteristics of Waves Generated by Polar Lows in Nordic and Barents Seas. *Remote Sens.* **2023**, *15*, 2729. https://doi.org/10.3390/rs15112729

Academic Editors: Sergei Badulin and Gad Levy

Received: 21 March 2023
Revised: 15 May 2023
Accepted: 22 May 2023
Published: 24 May 2023

1. Introduction

High-latitude intense mesoscale low pressure systems, named polar lows (PLs), or polar depressions, form during cold air outbreaks over the "warm" water surface in both hemispheres. These systems usually have typical spatial scales of 100–1000 km, near-surface winds of at least 15 m/s, horizontal translation speed around 10 m/s (2–23 m/s) and exist from several hours to a couple of days [1–4]. PLs can affect the climate system through the strong heat fluxes from the ocean surface to atmosphere [5,6] and play an important role in large-scale ocean circulation [7]. Severe winds and PL-generated waves pose threats to coastal and island infrastructure, vessels, offshore drilling platforms and even human lives.

The most active PLs develop in the Northern Hemisphere in winter, from October to April, over the ice-free areas with large air–sea temperature differences, such as the Norwegian, Barents and Labrador Seas [8]. The weaker intensity of PLs in the Southern Hemisphere is explained by smaller difference between the air and the sea surface temperature near the sea ice margin in the Antarctic compared to the Arctic and sub-Arctic areas. Marine cold air outbreaks are less intense and less frequent in the Southern Hemisphere [9].

The main criteria to differentiate PLs from other types of cyclones are based on their size, intensity, lifetime and parameters of atmosphere static stability, see overview in [10]. In the detection and tracking of PLs in reanalysis and atmospheric models, the number of detected PLs is rather sensitive to the choice of the range for these parameters. Due to different selection of PL identification criteria, there are still disagreements regarding certain parameters, such as the PL frequency [11]. The first analysis of global PL climatology using multi-decade reanalysis data was performed by Stoll et al. [8], who applied a storm tracking algorithm to ERA-Interim [12] and the Arctic System Reanalysis [13]. The authors suggested the most reliable criterion based on the tropopause wind speed poleward of the system and the difference in the potential temperature between the sea surface and the 500 hPa level. The authors compared their results with PLs parameters detected using subjective methods using infrared satellite imagery [14], passive microwave measurements [3] and data from synoptic weather stations [15]. The comparisons are quite consistent, yet PL density is underestimated compared to that listed in the data sets. This confirms an earlier conclusion [16–19] that the methods based on global atmospheric reanalysis cannot recognize all PL cases detected with subjective methods.

In the present study, the objective is to derive the spatial distributions of PL-generated surface waves of different height and wavelength using PL statistics based on satellite observations. Despite the relatively small horizontal scales of PLs, their strong winds can still lead to the development of very high waves. This is due to the effect of the enhanced fetch/duration of wave development in moving weather system. Waves propagating in the direction of PL heading (cyclone right–front sector in the Northern Hemisphere) do not rapidly leave the storm area and continuously grow, if their group velocity becomes close to the PL translation speed. The phenomenon of such a strong wave intensification, also known as the group velocity (quasi-) resonance, wave trapping or extended fetch effect, is well-known and has been extensively investigated for tropical cyclones (TCs) [20–24]. In PLs this effect is also observed [25–27], leading to abnormal high waves, with significant wave height (SWH) about 6 m on average, and up to 10–12 m in some cases, as registered during in situ observations [28,29].

Orimolade et al. [26] estimated the SWHs for 155 PL situations in the Norwegian and Barents Seas. These authors considered the extended fetch concept and a one-dimensional parametric model, first suggested by Bowyer and MacAfee [21]. Significant wave heights could then reach 9 m due to extended wave development. Considering two PL cases occurring close to the location of the platform with available wind and wave measurements, the authors conclude that the extended fetch phenomenon cannot always be well-captured by operational forecasting models, possibly resulting in the large underestimation of modeled SWH during PL events.

Due to the typically limited PL lifetime and space–time non-stationarity, Kudryavtsev et al. [27] recently argued that wave parameterizations based on the extended fetch approach, previously developed for TC conditions, cannot be directly applied to PL cases. Instead, an extended duration concept for wave development under PLs was suggested to provide first-guess estimates of wave parameters, depending on PL duration, spatial scale, wind speed and translation velocity. This concept and the expressions suggested in [27] are applied in this study to estimate the height and wavelength of PL-generated waves. The present work is a revision of the probability estimates, presented earlier in [30], where the calculations were based on stationary solutions of the parametric model of wave generation by a moving cyclone [23], i.e., on the extended fetch concept. Now, the restrained time-scales of short-living polar storms are accounted for, as well as spatial variability of PL emergence in Northern seas, which was considered uniform in [30].

The structure of the paper is as follows: the PL climatology to derive wave probability distributions is presented in Section 2; the model of wave generation and calculation procedure are described in Section 3; the results are presented in Section 4; then, a discussion of prediction accuracy and method constraints follows in Section 5; Section 6 concludes the study.

2. Data: PL Climatology

Polar-orbiting satellite observations are the main sources of observational data at high latitudes, particularly over the ocean [10]. The data used in the present study include areas and frequencies of PL formation in the Norwegian and Barents Seas and histograms of PL main characteristics (diameter, lifespan, propagation velocity and direction and traveled distance) obtained using subjective analysis applied to satellite measurements [3,31].

Spatial distributions of the locations where PLs were first detected, treated here as PL origins (Figure 1a), were taken from one of the most extensive datasets on PL climatology compiled from observation of 637 cyclones during 14 seasons, presented by Smirnova et al. [3]. To recognize the PLs, the authors visually analysed total water vapour content fields retrieved from brightness temperature measured using a Special Sensor Microwave Imager (SSM/I) on board the DMSP F13 spacecraft. Detected PL-like vortices were defined as PLs only if they contained at least 2 kg/m^2 of integrated water vapour, their sea surface wind speed exceeded 15 m/s as estimated from SSM/I and if the presence of cloud signatures was confirmed by thermal infrared imagery from Advanced Very High Resolution Radiometer (AVHRR). The data were collected for the Nordic and Barents Seas from September 1995 to April 2009. The authors also determined the dominant PL characteristics, i.e., their temporal and spatial distributions, including diameter, distance traveled, lifetime and speed of propagation. First presented in [3], these parameters were further converted to the mean annual number of cases (Figure 1c–e).

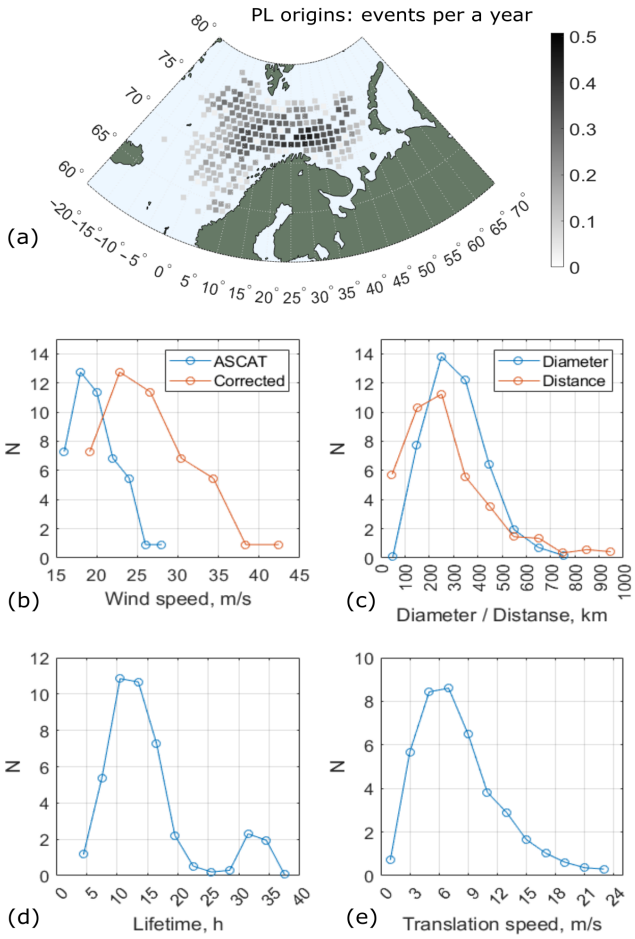

Figure 1. Statistical distributions of PL parameters: (**a**) mean annual spatial distribution of PL origins in 75 × 75 km grid cells [3]; (**b**) mean annual distribution of maximum wind speed from ASCAT [31] and its correction suggested by Polverari et al. [32], Equation (1); (**c**) mean annual distributions of PL diameter and traveled distance; (**d**) lifetime and (**e**) translation speed; data taken from [3].

Smirnova et al. [3] did not provide the distribution of wind speed in the observed cyclones. This distribution was taken from a more recent dataset collected by Golubkin et al. [31], where 131 PLs over the North Atlantic during 3 years were identified in Moderate Resolution Imaging Spectroradiometer (MODIS) infrared imagery, and their intensity was assessed using Advanced Scatterometer (ASCAT) data. Scatterometers are undoubtedly one of the most valuable instruments to routinely provide vector wind fields over the oceans, including polar latitudes. Yet, their current horizontal resolution is not high enough to capture strong wind gradients observed in PLs [33]. Precise wind speed estimation in extreme weather conditions may also remain challenging due to signal saturation in radar backscatter measurements at high winds [34]. Performing an indirect SFMR (Stepped-Frequency Microwave Radiometer), buoy and scatterometer data intercomparisons, Polverary et al. [32] suggested an expression to correct ASCAT wind speed U_{10A} for winds higher than 12 m/s:

$$U_{10} = 0.0095U_{10A}^2 + 1.52U_{10A} - 7.6. \quad (1)$$

The mean annual number of PL events with maximum wind speed lying within given 3 m/s ranges, obtained by [31] (blue line) and corrected using (1) (red line) are plotted in Figure 1b.

Distributions of PL propagation direction were studied by Rojo et al. [4] using images acquired from AVHRR during 14 seasons in the Nordic Seas. Generally, the direction of PL movement is controlled by the large-scale flow in the lowest atmospheric layers and differs according to weather regimes (e.g., phase of North Atlantic Oscillation). It was found that the vast majority of PLs travel southward or southeastward; however, a substantial number of PLs propagate westward and even northward. The observed PL directional distribution, obtained in [4], was approximated by [30] in terms of probability P_ϕ of PL propagation in a direction $\phi \pm \Delta\phi/2$:

$$P_\phi = \Delta\phi \cdot 0.47\exp[-0.66(\phi - \phi_m)^2], \quad (2)$$

where $\phi_m = -\pi/4$ is the mean direction for the entire ensemble of PLs moving generally southeastward, ϕ and $\phi - \phi_m$ are defined in the range $[-\pi, \pi]$ and P_ϕ satisfies the condition $\int_{-\pi}^{\pi} P_\phi \Delta\phi = 1$; hereinafter, angles are counted counterclockwise from the East direction.

3. Method

3.1. Model of Wave Evolution

The listed PL statistical distributions are further used to assess the wave fields, generated by these PLs, using empirical relations for wave development, first suggested by Kitaigorodskii [35] and justified in a number of experimental and theoretical studies [36–38]. Suggested and verified, the wave energy e and the spectral peak frequency ω, scaled by the local wind speed u and gravity g, follow the self-similar power laws, known as fetch-limited,

$$\begin{aligned} eg^2/u^4 &= c_e(Xg/u^2)^p \\ \omega u/g &= c_a(Xg/u^2)^q, \end{aligned} \quad (3)$$

and duration-limited,

$$\begin{aligned} eg^2/u^4 &= c_{et}(tg/u)^{p_t} \\ \omega u/g &= c_{at}(tg/u)^{q_t}, \end{aligned} \quad (4)$$

laws for wave development under uniform wind conditions. In Equations (3) and (4), X and t are fetch and time of wave development, respectively; c_e, c_a, p, q, c_{et}, c_{at}, p_t, q_t are empirical constants, related as [23,39]:

$$q_t = q/(1+q),$$
$$p_t = p/(1+q),$$
$$c_{et} = c_e[(1+q)/2c_a]^{p_t},$$
$$c_{at} = c_a[(1+q)/2c_a]^{q_t}.$$

Following Kudryavtsev et al. [40], the fetch-limited constants are: $c_e = 1.3 \times 10^{-6}$, $c_a = 11.8$, $p = 3/4$, $q = -1/4$, and thus, the duration-limited constants are: $c_{et} = 4.13 \times 10^{-8}$, $c_{at} = 37.25$, $p_t = 1$, $q_t = -1/3$.

In a number of studies [20,21,23,24], relations (3) were successfully applied for simulations of waves generated by TCs. For such cases,"physical" fetch X is replaced by an "enhanced" ("effective", "extended") fetch, which takes into account the moving nature of the TC, to become a function of TC parameters: radius, wind speed and translation velocity. Yet, as demonstrated by Kudryavtsev et al. [27], an extended fetch concept, originally developed for TC and applied to PLs, generally overestimates surface wave heights compared to satellite altimeter observations.

Using semi-empirical relationship for extended fetch suggested in [24], their Equation (18), Kudryavtsev et al. [27] provided a relation for the duration, t_{max}, of wind waves development in TC/PL wind field moving with translation velocity V and characterized by maximum wind speed u_m and its radius R_m. The physical meaning of t_{max} is the time required for the waves to reach the maximal possible values of energy/wavelength, prescribed by the extended fetch laws. This time-scale reads:

$$t_{max} = t_0[l_\lambda + m_\lambda(R_m/L_{cr})^{n_\lambda}]^{-1/(2q_t)}, \quad (5)$$

where t_0 is the time scale of wave development for a stationary storm,

$$t_0 = u_m/g(c_a/c_{at})^{1/q_t}(R_m g/u_m^2)^{q/qt}, \quad (6)$$

$[l_\lambda, m_\lambda, n_\lambda] = [1, 1.37, -0.38]$ for $R_m/L_{cr} >= 1$ ("slow" cyclones, as termed in [24]) and $[l_\lambda, m_\lambda, n_\lambda] = [0, 1.67, 0.31]$ for $R_m/L_{cr} >= 1$ ("fast" cyclones); L_{cr} is the distance from the initial point of wave train generation to the turning point, where the projection of the wave group velocity on the cyclone heading becomes equal to its translation velocity ("group velocity resonance") [23]:

$$L_{cr}g/u^2 = c_{cr}(u_m/2V)^{1/q},$$

c_{cr} is linked to the fetch laws constants as $c_{cr} = -c_\alpha^{-1/q}q/(1+q) = 6.5 \times 10^3$.

Values of t_0 and t_{max} are plotted in Figure 2 versus PL translation velocity for the cases of u_m = 15, 25, 35 m/s for a typical PL diameter of 300 km. Using Equations (5) and (6), the time, for a moving PL, to reach a stationary (steady) solution increases up to 3 times compared to a stationary case ($V = 0$). Maxima occurred for cyclones whose parameters satisfy the condition of full group velocity resonance, $L_{cr} = 1$, which is fulfilled at each peak of the curves.

The colour indicates joint probability of emergence of PL prescribed with given lifetime T_{life} and translation velocity V. An important feature is that the maximum of the probability distribution, which is around the point $T_{life} = 13$ h and $V = 7$ m/s, is located mainly below the curves (5). As found, a substantial part of PLs (60–70%, depending on specified u_m and R_m) have a lifetime which is less than the time-scale t_{max} required for waves to reach a maximal possible development under moving TC/PL predicted by steady extended fetch solutions. Hence, the wave development in PLs should rather be considered within the framework of duration-limited laws (4), instead of extended fetch ones initially used in [30].

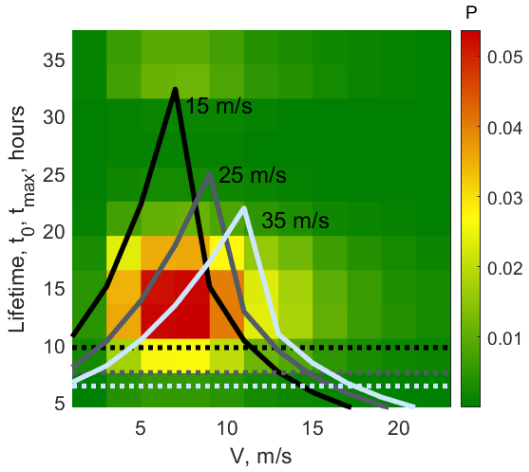

Figure 2. Color: joint probability of PL lifetime and translation speed. Dotted lines: time of wave development to reach a steady solution in a stationary, Equation (6), and (solid lines) moving, Equation (5), cyclone with diameter 300 km and maximum wind speed 15, 25 and 35 m/s (white, grey and black lines correspondingly.

In terms of significant wave height H and wavelength L, Equation (4) applied to PLs, reads:

$$H = 4u_m^2/g \cdot c_{et}^{1/2}(tg/u_m)^{p_t/2}$$
$$L = 2\pi u_m^2/g \cdot c_{at}^{-2}(tg/u_m)^{-2q_t}. \quad (7)$$

The generation of PL results from the instability of the background air flow. Therefore, already at the beginning of the evolution, the sea surface under a PL is "filled" with wind waves. To a first guess, the significant wave height and wavelength of these waves correspond to parameters of the waves generated under stationary PL with the same radius and wind speed. To introduce this initial condition, we assume that at the moment of PL formation, parameters of waves are given by (7) at $t = t_0$ defined by (6).

If $t_0 + T_{life}$ is larger than t_{max} defined by (5), the waves in PL develop in time according to (7) until $t = t_{max}$. At $t = t_{max}$, H and L described by (7) take the values which correspond to the extended fetch laws (see Equation (2) from [27]), which further remain constant during the final stage of PL evolution, i.e., at $t_{max} < t < T_{life} + t_0$.

If the PL lifespan T_{life} is smaller than $(t_{max} - t_0)$, parameters of waves in PL attain the values defined by (7) with $t = t_0 + T_{life}$ which are apparently smaller than the values predicted by the extended fetch laws, i.e., the waves cannot reach the maximum possible SWH and wavelength corresponding to a given PL with parameters u_m, R_m and V.

After $t = t_0 + T_{life}$, the waves turn to swell regime, attenuating with distance l, as suggested by Yurovskaya et al. [41,42]:

$$(H_i/H_{sw})^4 = 1 + \pi^5/2\epsilon_T^4 \cdot H_i^4 L_i^{-5} l$$
$$(L_{sw}/L_i)^5 = 1 + a\ln[1 + \pi^5/2\epsilon_T^4 \cdot H_i^4 L_i^{-5} l], \quad (8)$$

where H_{sw} and L_{sw} are SWH and wavelength of swell waves, respectively; H_i and L_i are initial swell parameters, i.e., H and L of wind waves at $l = 0$ and $t = t_0 + T_{life}$ (equal to that at $t = t_{max}$, if $t_0 + T_{life} > t_{max}$); $\varepsilon_T = 0.4$ is the threshold wave steepness defining the process of wave breaking; $a = 0.15$ is the constant absorbing other constants of the 2D parametric model [40].

Effects of wave rays focusing/defocusing are omitted in (8), taking into account only wave dissipation due to wave breaking (see Appendix A.3 of [41] and Section 2.2.1 of [42] for more details).

The self-similar model considered above is the 1D model of wave growth. Further, we apply this model for the waves generated in the right sector where the effect of wave trapping is expected to result in the possible generation of the highest waves. Indeed, numerical simulations of waves inside TCs using the 2D parametric model [24] (e.g., Figures 6–8 and 10 of [24]) show that most intense waves are formed to the right of TC center relative to the heading, within an area with horizontal scale about $2R_m$. These intense waves further propagate as swell in the cyclone heading direction, or are left behind moving cyclone, depending on their group velocity compared to cyclone heading speed. Waves generated in directions different from the PL heading are neglected here.

3.2. Examples of Model Performance

To illustrate the performance of the self-similar model described in the previous section, two PL cases are considered. The outputs of ERA5 ECMWF reanalysis [43] (10 m height wind speed and SWH) are taken here as reference fields.

The first case, further termed PL#1, has been already studied in [27], where self-similar properties of its generated waves were demonstrated using altimeter measurements and 2D parametric model simulations (Section 3 and Figure 7 of [27]). We consider evolution of this PL starting from 20 January 2017, after it changed its heading direction from East to South-East, with higher wind speeds in the right PL sector (Figure 3a–d).

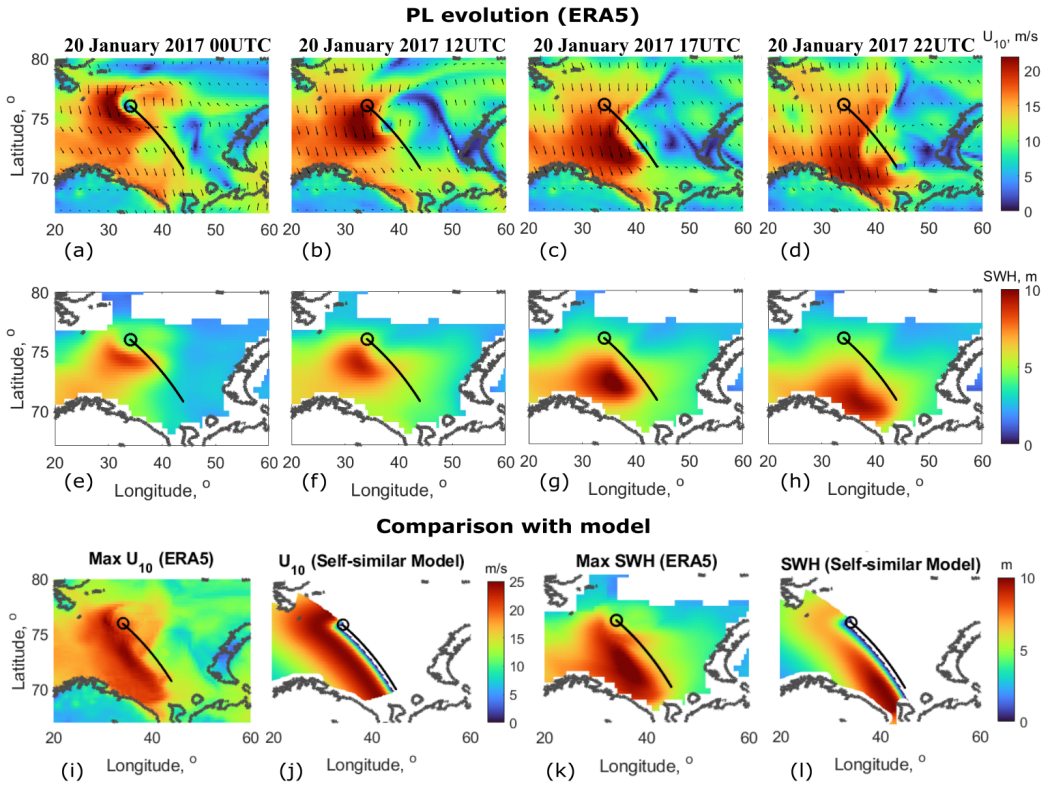

Figure 3. ERA5 fields of (**a**–**d**) wind speed and (**e**–**h**) SWH during PL#1 lifetime. Maximum (**i**) wind speed and (**k**) SWH observed at every point during the PL lifetime. Self-similar model (**j**) wind speed for PL#1 and (**l**) SWH obtained using Equations (7) and (8). Black solid lines mark the PL trajectory; black circle is the PL origin.

According to ERA5 data, (Figure 3e–h), waves reached high values, about 10 m, in the afternoon, half a day after the PL started moving in constant direction. Figure 3i,k show the ERA5 output in terms of the maximum values of the wind speed and SWH fields, respectively, at each grid point during the evolution of PL#1. The wind and SWH fields of PL#1 exhibit pronounced bands of strong wind and high waves to the right of the trajectory.

Figure 3j,l show the wind and SWH fields (again, maximum values during the whole observation time), respectively, produced by the simplified self-similar model. The wind radial distribution follows a Holland function [44], with $u_m = 25$ m/s, $R_m = 350$ km and shape parameter $B = 1$. As suggested in the simplified model, waves develop under constant wind forcing during the PL lifetime only in the its right sector where the wind direction is aligned with the PL heading. Calculations of SWH (Figure 3l) were carried out according to Equations (7) and (8) with t estimated as $t = \min(t_{max}, T_{life} + t_0, D/V + t_0)$, D the distance from PL origin, $T_{life} = 24$ h and $V = 9$ m/s and u_m equal to local radial wind speed. The simplified self-similar model calculations are comparable to ERA5 output (Figure 3k) both in magnitude and spatial behaviour.

Another case, PL#2, occurred on 30–31 January 2011, also in the Barents Sea. It moved in east–south–east direction with mean velocity of 8 m/s and changed its direction to the southward at the final stage (Figure 4a–d). Although the shape of its wind radial profile is more symmetrical than PL#1 (compare Figures 3i and 4i), the highest waves are still observed to the right of the PL trajectory where the wave group velocity resonance is expected (Figure 4e–h).

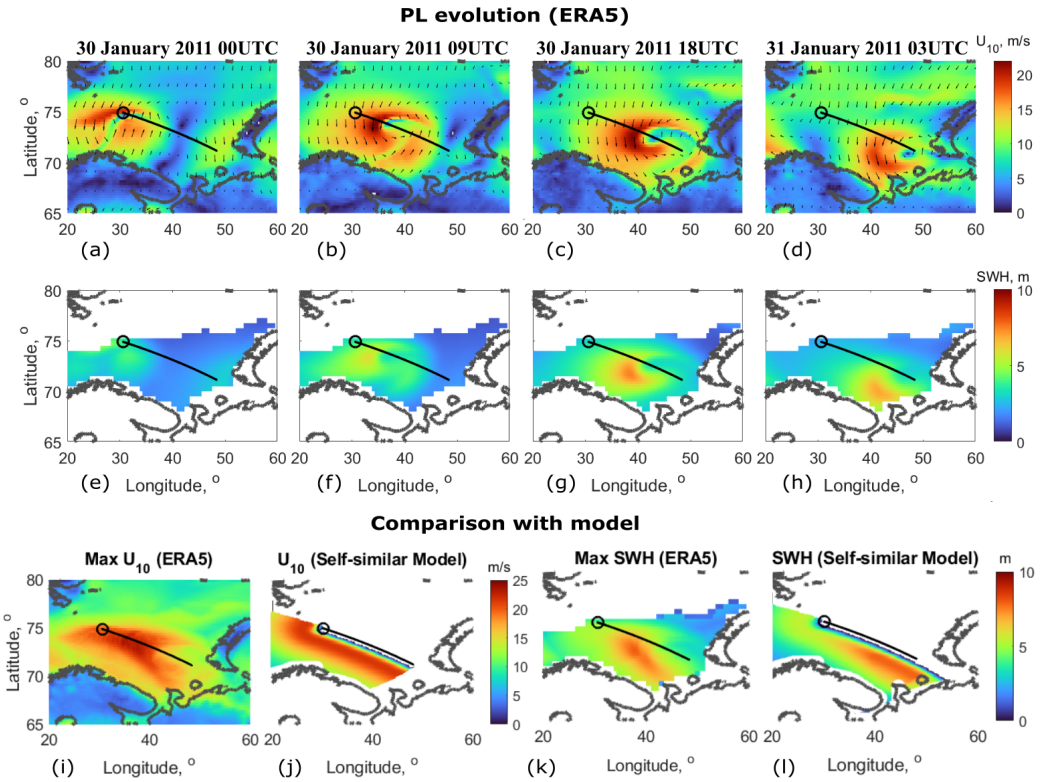

Figure 4. ERA 5 fields of (**a**–**d**) wind speed and (**e**–**h**) SWH during PL#2 lifetime. Maximum (**i**) wind speed and (**k**) SWH observed at every point during the PL lifetime. Self-similar model (**j**) wind speed for PL#2 and (**l**) SWH obtained using Equations (7) and (8). Black solid lines mark the PL trajectory; black circle is the PL origin.

Self-similar model simulations for PL#2 with $R_m = 300$ km, $u_m = 21$ m/s, $V = 8$ m/s and $T_{life} = 27$ h give the values of SWH, again consistent with ERA5, though slightly overestimated near the shore, where PL changed its direction and lost intensity (Figure 4k,i).

Despite the quite rough assumptions concerning the wind conditions and the region of wave development, the presented case studies show the highest waves are well-captured by self-similar model. The resulting SWH spatial distributions are adequate enough to further consider the ensemble of solutions to estimate wave height probabilities. To further simplify the calculation procedure, we set the SWHs and wavelengths to be constant within $2R_m$ distance in the cross-track direction with values defined by (7) and (8).

3.3. Calculation Procedure

To assess the probability of waves reaching given threshold values at a given location, all possible situations of PL propagation characteristics are considered.

According to data presented in [3], about 45 PLs yearly form in points (x_i, y_i) marked with gray squares in Figure 1a: 0.1–0.5 cases per point, on average. We suppose that each of these cyclones can have arbitrary (assuming constant during T_{life}) values of u_m, R_m and V in the ranges of their distributions (Figure 1b–e) and can propagate in any direction.

Summing up all these situations, the total annual number of events of PL-generated waves observed in point (x_0, y_0) is

$$N_0 = \sum_{i,j,k,m,n} N^i \cdot P_\phi^i \cdot P_u^j \cdot P_R^k \cdot P_V^m \cdot P_T^n, s \tag{9}$$

where N^i is the annual number of PL origins in each of the points (x_i, y_i); P_u^j, P_R^k, P_V^m and P_T^n are the probabilities of PL maximum wind speed u_m^j, radius R_m^k, translation velocity V^m and life timeT_{life}^n, respectively, obtained from distributions presented in Figure 1b–e, to fulfill the conditions: $\sum_j P_u^j = 1$, $\sum_k P_R^k = 1$, $\sum_m P_V^m = 1$ and $\sum_n P_T^n = 1$; P_ϕ^i is the probability of a PL originated in point (x_i, y_i) to move in the direction of point (x_0, y_0).

To estimate P_ϕ^i with Equation (2), the value of ϕ and the angular range $\Delta\phi$ must be defined. Neglecting the waves generated in directions different from the PL heading direction, the highest waves, propagating within the area of size $2R_m$ to the right of PL trajectory, will pass through a point (x_0, y_0), if the PL heading direction ranges from ϕ_0 to $\phi_0 + \Delta\phi$, where $\phi_0 = \arctan[(y_i - y_0)/(x_i - x_0)]$, $\Delta\phi = 2\arctan(R_m/D)$, D is the distance between point of the PL generation and point (x_0, y_0), $D = \sqrt{(x_i - x_0)^2 + (y_i - y_0)^2}$. Probability P_ϕ^i is then

$$P_\phi^i = 0.47 \int_{\phi_0}^{\phi_0 + \Delta\phi} \exp[-0.66(\phi - \phi_m)^2] d\phi.$$

The calculation procedure consists of the following steps:

- The wave parameters for each of $(i \cdot j \cdot k \cdot m \cdot n)$ terms of (9) are first predicted by Equation (7) with $t = \min(t_{max}, T_{life} + t_0, D/V + t_0)$.
- If the distance traveled by the PL, $T_{life}V$, is less than the distance D adjusted for $2R_m$ (as mentioned above, the area covered by the most developed waves has a scale of approximately $2R_m$): $T_{life}V < D - 2R_m$, then the waves reach the point (x_0, y_0) as swell with parameters prescribed by Equation (8), with $l = D - 2R_m - T_{life}V$ and H_i, L_i obtained at $t = \min(t_{max}, T_{life} + t_0, D/V + t_0)$.
- If the PL track is masked by the land, the term $(N^i \cdot P_\phi^i \cdot P_u^j \cdot P_R^k \cdot P_V^m \cdot P_T^n)$ is set to zero (ice coverage is not considered in present study).
- The result of wave parameter calculation at each iteration is compared with each of the specified threshold values in the range from 2 to 15 m for SWH and from 100 to 500 m for wavelength. If H or L exceeds a given threshold, the respective number of events, $(N^i \cdot P_\phi^i \cdot P_u^j \cdot P_R^k \cdot P_V^m \cdot P_T^n)$, is summarized with the number accumulated at earlier iterations for this threshold.
- Finally, the total annual numbers of cases of occurrence the waves with SWH and wavelength exceeding specified levels are obtained for each of the 75 × 75 km grid points (x_0, y_0).

4. Results

4.1. Significant Wave Height Probability Distributions

Spatial distributions of the annual number of events, associated with PLs, with SWH greater than 2, 4, 6, 8, 10 and 12 m, are presented in Figure 5. The probability fields are qualitatively similar. The region in the vicinity of the North of the Scandinavian peninsular,

is where high waves are likely the most frequently observed. The Greenland Sea and the South of Norwegian Sea are apparently less affected by PLs and PL-generated waves. Waves higher than 4–6 m occur 5–6 times a year at any point of the East of Norwegian Sea and South of Barents Sea; waves larger 8–10 m appear 1–2 times a year, and SWHs greater than 12 m can appear once in several years. The frequency of appearance of 15 m waves associated with PLs is less than once in 10 years (not shown).

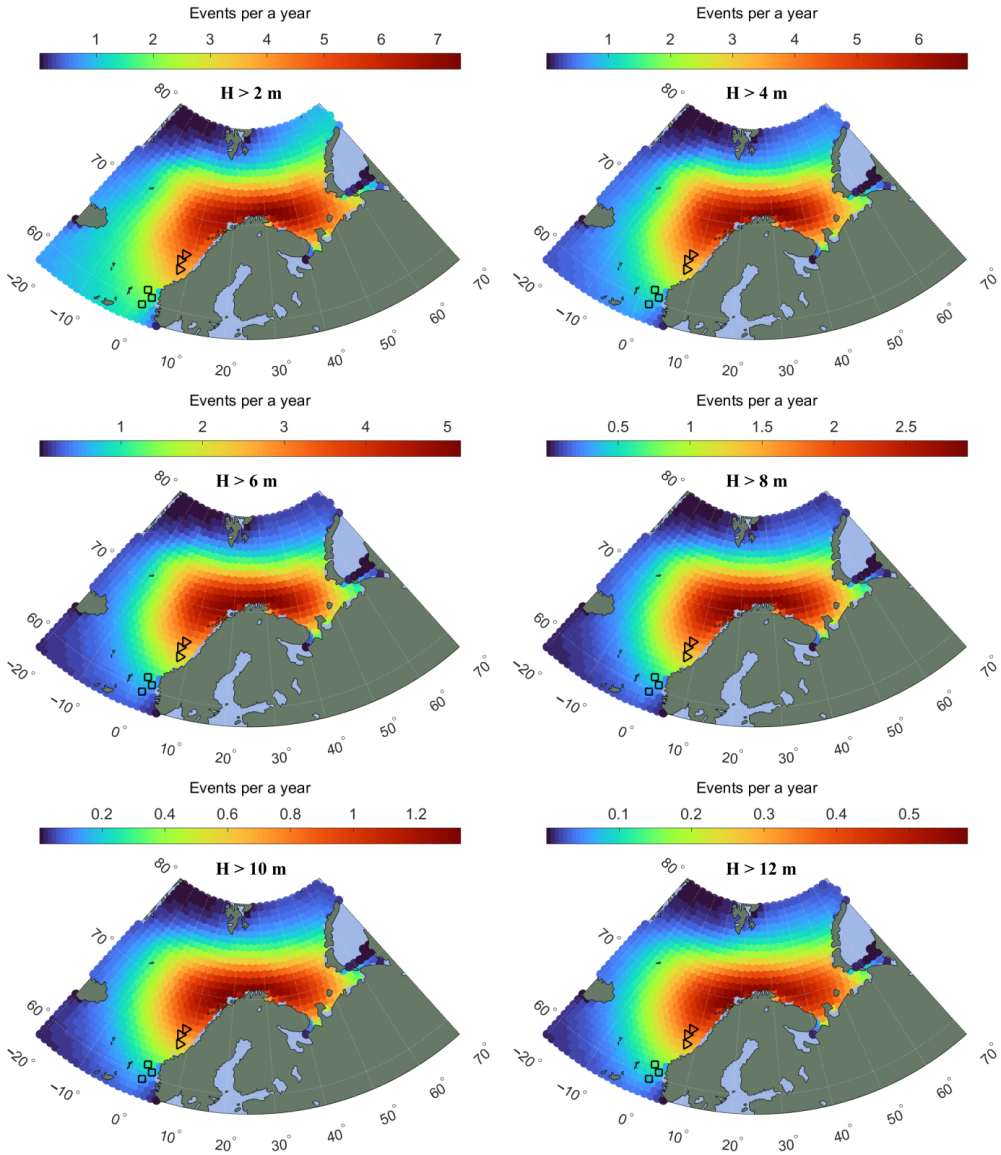

Figure 5. Spatial distribution of the annual number of events when SWH of PL-generated waves exceeds the specified threshold values: 2 m, 4 m, 6 m, 8 m, 10 m and 12 m. Black triangles are location of maritime stations 76,925, 76,928 and 76,930; squares are stations 76,923, 76,931 and 76,932.

The probability of events at given points are independent of grid resolution, should be noted. However, the total number of events cannot be estimated by summing up the events in the grid cells, because SWHs in neighbour points are often correlated, being affected by the same PLs.

The obtained SWH probability distributions agree in order of magnitude with those previously derived by Kudryavtsev et al. [30], who used extended fetch laws (instead of extended duration ones) for waves generated by PLs. Note that Kudryavtsev et. al used smaller wind speeds, in the range 15–33 m/s vs. 19–43 m/s in the present study. Shown below in Section 5.1, the application of duration-limited laws for less intense winds

provides much lower occurrences of high waves compared to estimates presented in Figure 5. Differences from [30] can also be related to the specification of the PL occurrence fields: in the present study, they are defined as reported by [3], while in [30], they are spatially uniform.

4.2. Comparison with Observations

The result can be directly compared with field measurements analyzed by Rojo et al. [28]. The data from eight maritime stations, providing wind speed, SWH, sea level pressure and water and air temperature, were collected during 14 winters, covering 29 cases of PLs identified manually from their associated cloud signatures on satellite imagery. Three of these stations (76,925, 76,928 and 76,930) are located in the Norwegian Sea around 65°N8°E and three in the North Sea around 60°N3°E (76,923, 76,931 and 76,932); the two groups are marked with triangles and squares in Figure 5, respectively. For these two groups of stations, the cumulative and mean annual number of the events of PL-generated waves exceeding the specified thresholds are listed in Table 1, which is based on the data from Table 2 of [28].

Table 1. Number of cases of PL-associated waves in two locations of maritime stations, data from Rojo et al. [28].

	Stations 76,925, 76,928, 76,930		**Stations 76,923, 76,931, 76,932**	
SWH Threshold	**Total Number of Events**	**Annual Number of Events**	**Total Number of Events**	**Annual Number of Events**
>2 m	22	1.6	6	0.43
>4 m	20	1.4	6	0.43
>6 m	12	0.86	4	0.29
>8 m	5	0.36	1	0.07
>10 m	1	0.07	1	0.07

In Rojo et al. [28] analysis, only one record per PL event was considered for every maritime station (in total, 95 records), and most of the 29 selected PLs affected the maritime conditions at more than one station at the same time. The data presented in Table 1 also include only one wave condition event per PL case, selected among the three stations of the group, i.e., the highest values of SWH registered by one of these stations during a PL passage.

For the group located in the Norwegian Sea, SWHs greater than 2 m and 4 m were observed for almost all PL situations, about 20 times, or 1.5 times per year on average; waves higher than 4 m occurred 12 times during 14 years, higher than 8 m–5 times, and 10 m waves were registered only once. For the second group of stations, the southern one, the frequency of high wave events is much smaller, being less than one event in 2–3 years for waves higher than 2–6 m, and again, only one case of SWH larger than 10 m occurred over the whole period of PL observations. Note that no PL-associated waves higher than 11 m were registered at any of these eight stations.

Though these data are qualitatively—and to some extent quantitatively (of order of magnitude)—consistent with the result presented in Figure 5, the model prediction generally overestimates the probability of high waves, as compared to in situ observations. Besides possible missing PL events in Rojo et al. [4,28] satellite data analysis (e.g., the authors of [4] obtained 14 cases yearly on average for Northern Seas, versus 45 cases yearly in the dataset [3] used in the present study), and omitting the PL-generated swell waves in that analysis, which can be still quite high outside the storm area, the present approach also contains assumptions and uncertainties which can lead to the overestimation of wave probabilities. This is further discussed in Section 5.

4.3. Wavelength Probability Distributions

Figure 6 presents spatial distribution of the annual number of cases when wavelengths of the PL-generated waves exceed 100, 200, 300 and 400 m. For relatively short waves, about 100 m in wavelength, the distribution qualitatively repeats that for SWHs: compare Figures 5 and 6a. As developed, the length of swell waves does not decrease, and even slightly increases with distance, in contrast to strong wave height attenuation, as shown in Equation (8). For the most intense PLs, this leads to the appearance of long (though not always too high) waves along the whole coastline from the west of Norwegian peninsular to the north of Novaya Zemlya, including the Pechora Sea (Figure 6b,c).

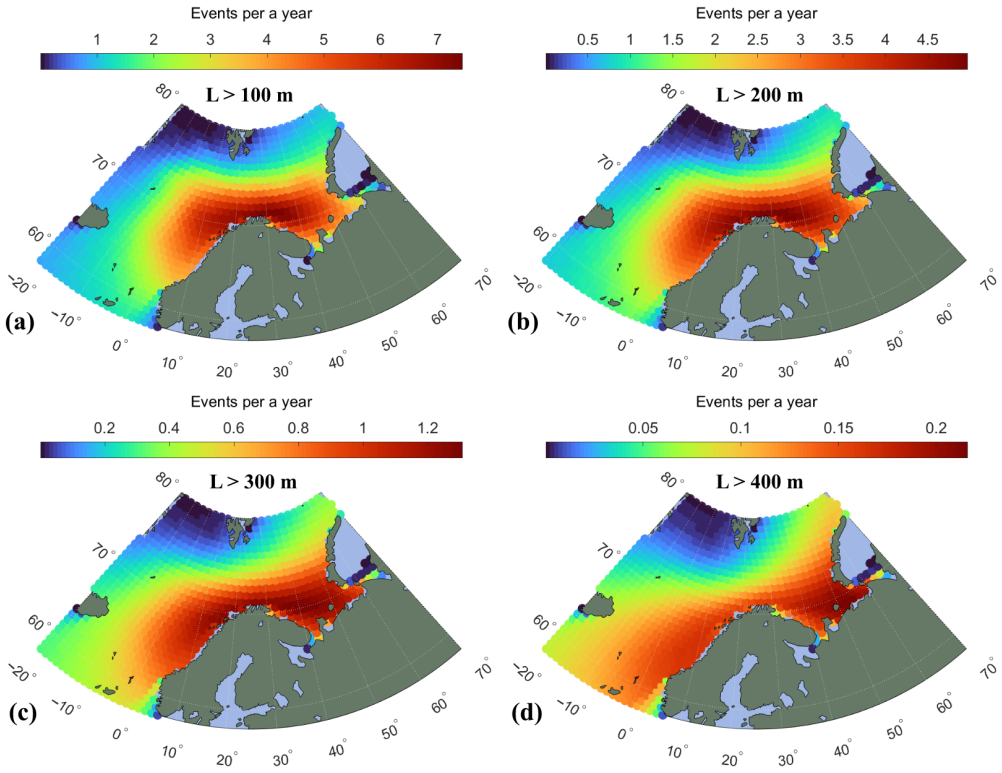

Figure 6. Spatial distribution of the annual number of events when wavelength of PL-generated waves exceeds the specified threshold values: 100 m, 200 m, 300 m and 400 m.

Waves from PLs with lengths larger than 100 m are predicted to appear up to 7 times a year, 200 m and larger waves occur 2–5 times a year, 300 m waves occur about once a year, and 400 m occur less than once in 5–10 years. The probability of 500 m wavelengths (not shown) is found to be very low—once in 50 years.

Such a small probability of waves longer than 400 m is indirectly confirmed by the recent study of Myslenkov et al. [45]. These authors present the information about wave climate in the Kara Sea based on numerical simulations using WAVEWATCH-III model to reconstruct wind wave fields for the period from 1979 to 2017. Although the Kara Sea is mostly shielded from the impact of PLs originating in the Barents and Norwegian Seas, the region to the West of Novaya Zemlya is also covered in Figure 7 of [45]. As reported, the largest wavelengths in the east of the Barents Sea for the 39 year period are about 300 m. The authors also mention the appearance of remnant swell events with an insignificant wave height and peak periods of up to 20 s. The maximum SWH obtained in that study (their Figure 8 and Figure 13) was 12 m, which is also in agreement with our prediction.

5. Discussion

5.1. Accuracy of Predictions

The presented probability maps were obtained using a number of assumptions that could affect the accuracy of the results, particularly leading to overestimation of the wave heights and wavelengths. The derived occurrence frequencies, especially for the highest and longest waves, should be treated as their upper estimates.

First, PLs are supposed to move in the same direction with constant heading velocity V and constant parameters u_m and R_m during the whole lifetime. In reality, all these parameters are very unstable, and the cyclone can abruptly change its propagation speed and direction.

Second, the cyclones are considered to have an axi-symmetrical shape, while the wind field in reality is usually asymmetrical. The strongest winds are typically located in right quadrant of the storm [10,28]. Yet, if the PL changes its direction, shifting the area of maximum winds, e.g., to the backward sector, the extended fetch/duration concept cannot be applied [27].

Wind speed u_m in PL is also of particular concern. The most representative PL climatology datasets [3,4] do not provide the wind speed distributions, while scatterometer-derived winds in the dataset of Golubkin et al. [31] are the maximum winds reached during the PL exposition. On one hand, the correction of scatterometer data towards higher values should be performed, as discussed in Section 2. However, on the other hand, the assumption that this maximum value remains the same during the whole PL lifetime may lead to strong overestimations of wave parameters. The measurements from Northland maritime stations [28] show that during 14 years of observations of the PL-associated winds, the wind speed only once reached the value of 31 m/s, while in the absolute majority of cases, it did not exceed 25 m/s.

In this context, Figure 7 presents the spatial distributions of SWH probabilities for the same thresholds as in Figure 5, but obtained for weaker winds, i.e., for ASCAT wind speed distributions on Figure 1b, not corrected using Equation (1). As a result, the annual number of cases of the largest SWHs decreases, particularly, down to several cases in 30 years for 10 m waves, compare Figure 5 and Figure 7. The values for 6 m and 8 m waves are now consistent with buoy observations [28] in the regions marked with triangles and squares in Figure 7. The probabilities of larger waves now seem underestimated, but note that buoy observation period (14 years) is not enough to reliably estimate the probabilities of events which occur once in decade or rearer. In any case, the result of the calculations using the present approach is shown to be very sensitive to the wind speed distribution, which should be more accurately specified to obtain more reliable estimates.

The other sources of uncertainties may consist in quite arbitrary selection of the size of the area of the most intense waves ($2R_m$ in present calculations), neglecting the waves propagating in directions different from PL heading, and assumption of independence of cyclone parameters, i.e., of equal probabilities for any of combinations of R_m, u_m, V and T_{life}, though some of them (e.g., cyclone size and intensity) can be generally correlated, as often observed for TCs [46–49]. Yet, these simplifications are apparently not crucial and do not lead to significant changes of the results, e.g., the variation of the size of the area of maximum waves from $1R_m$ to $3R_m$ gives probabilities comparable to those obtained for $2R_m$.

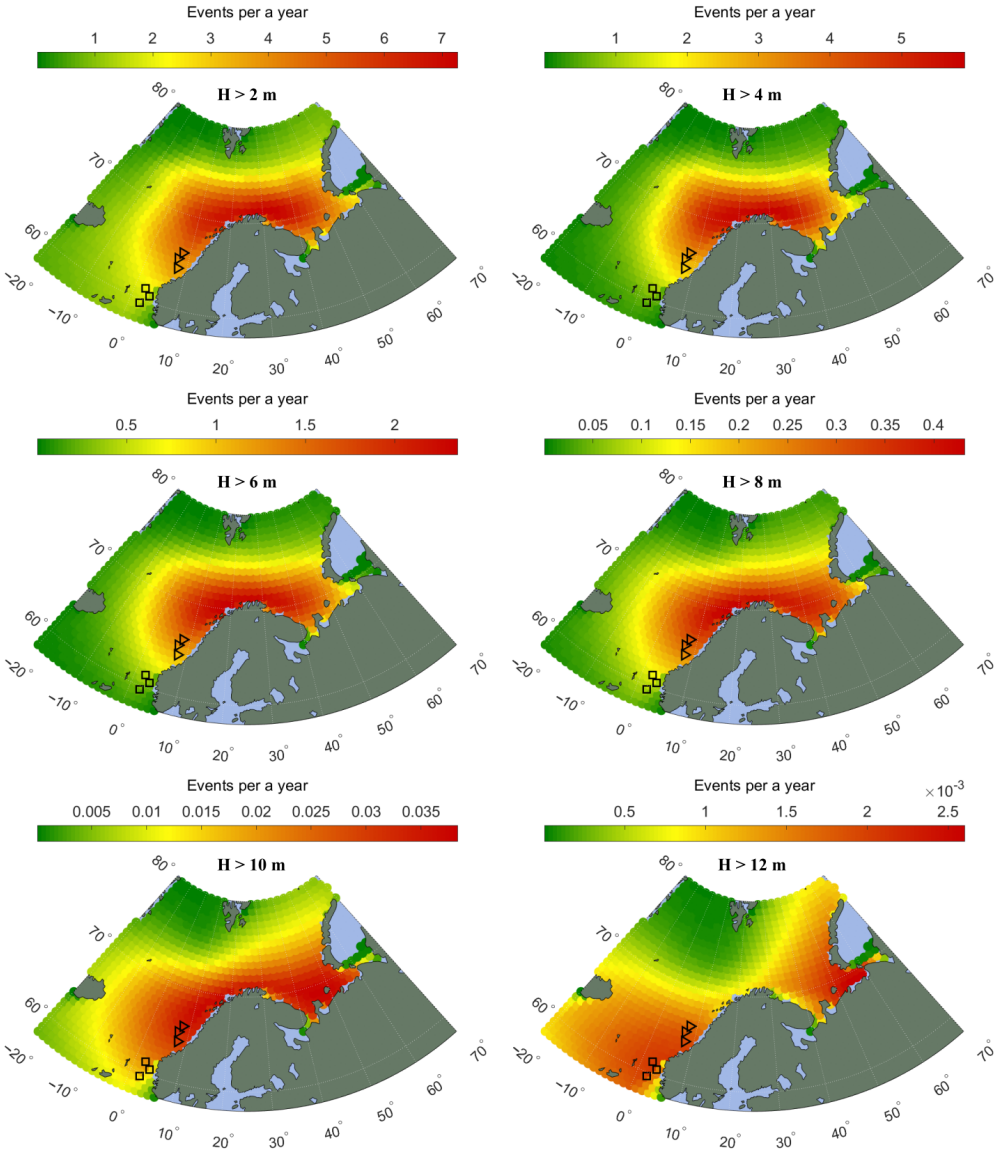

Figure 7. Spatial distribution of the annual number of events when the SWH of PL-generated waves exceeds the specified threshold values: 2 m, 4 m, 6 m, 8 m, 10 m and 12 m. Black triangles are location of maritime stations 76,925, 76,928 and 76,930; squares are stations 76,923, 76,931 and 76,932. The calculation using the wind distribution without correction of scatterometer data.

5.2. Waves Not Associated with PLs

Though PLs are a major factor to generate the highest and the most dangerous waves, mature sea states are also often related to strong winds without forming the cyclonic structures.

Figure 8a demonstrates the annual probability of wind speed exceeding 15 m/s, as estimated from 11 years of reanalyses (ERA5 wind field daily product from 2012 to 2022). The frequency of occurrence of such events in the Barents and Norwegian Seas is 20–50 cases (days) in a year, while PL-associated winds are observed less than 5 times a year, as obtained from PL parameters distributions (Figure 8b). The latter probabilities were estimated using the similar way as described in Section 3.2, with the expression for the annual number of PL passages through a given location (x_0, y_0):

$$N_0 = \sum_{i,j,k} N^i \cdot P_\phi^i \cdot P_R^j \cdot P_{Dist}^k, \quad (10)$$

where N^i is the annual number of PL origins in each of the points (x_i, y_i) shown in Figure 1a; P_R^j, P_{Dist}^k are the probabilities of iterated PL radii and PL traveled distances; P_ϕ^i is the probability (2) of PL propagation in the direction of point (x_0, y_0) within the angular sector $d\phi = 2R_m/D$, $D = \sqrt{(x_i - x_0)^2 + (y_i - y_0)^2}$; $N^i \cdot P_\phi^i \cdot P_R^j \cdot P_{Dist}^k = 0$, if the distance traveled by PL is less than $D - R_m$.

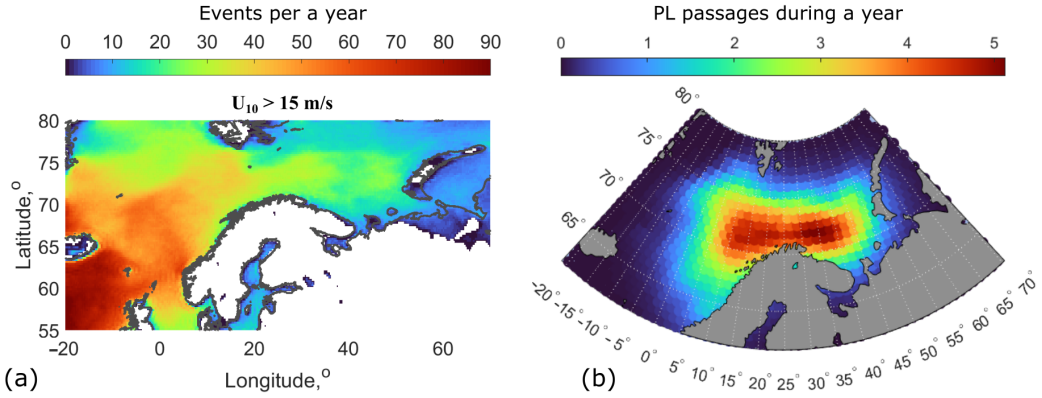

Figure 8. (**a**) Spatial distribution of the annual number of days when maximum wind speed exceeds 15 m/s, estimated from ERA5 for 2012–2022. (**b**) Spatial distribution of the annual number of PL passages in a given point.

Spatial distributions of the annual number of PL cases using Equation (10) are qualitatively and quantitatively consistent with the PL track density, i.e., the number of storms within a radius of 100 km, calculated by Romero and Emanuel [50] from the reanalyses (ERA-Interim and NCEP–NCAR) and from the set of numerical models. These authors (see their Figure 5 in [50]) obtained about 200 cases per century for the region to the north of Scandinavian peninsular, slightly less than the values presented in Figure 8b. This is still fairly tolerable, considering the typical PL density underestimation inherent to the methods based on numerical simulations and reanalysis.

The comparison of the subplots in Figure 8a,b clearly demonstrates the importance of accounting for non-PL high wind conditions in estimating the probabilities of abnormally high wave occurrences. Although this will be the scope of future investigations, the first-guess results can be obtained directly from ERA5 SWH reanalysis for the same period: 2012–2022. The maps of annual number of days when SWH of waves, either related to PLs or of any other nature, exceeded specified threshold values, are presented in Figure 9. As compared to Figure 5, the occurrence of waves with heights up to 4 m is greatly exceeds that predicted for pure PL conditions. The probabilities of 6 m waves are comparable in the Barents Sea, but 10 times higher in ERA5 data in the Norwegian Sea, while waves higher than 8 m appear several times a year according both to ERA5 and the present study results. This confirms that abnormally high and the most dangerous waves in the Barents and the north of Norwegian Seas are related to PL events, while the extreme wave conditions in the south of the Norwegian Sea are, rather, determined by other factors.

Recent advances in ocean remote sensing—particularly synthetic aperture radar (SAR) high-resolution multi-polarization measurements, such as those from satellites Sentinel-1, RADARSAT-2 and TerraSAR-X—further open new opportunities to study the propagation of ocean waves in the Arctic seas, covering vast areas continuously, independent of the weather and time of day. SAR data allows the determination and monitoring of wave characteristics, including peak wavelength, energy and direction, and also within sea ice, in addition to the study of wave–ice interactions in the the marginal ice zone [51–53]. The SWIM (Surface Waves Investigation and Monitoring) instrument onboard the CFOSAT (China France Oceanography Satellite) has also been demonstrated to be another efficient source of quantitative evidence for the wavelengths and directions of waves generated by polar storms [54]. In this context, the presented wavelength and wave height probabilities

can be improved and further validated using these new satellite sources of ocean wave properties.

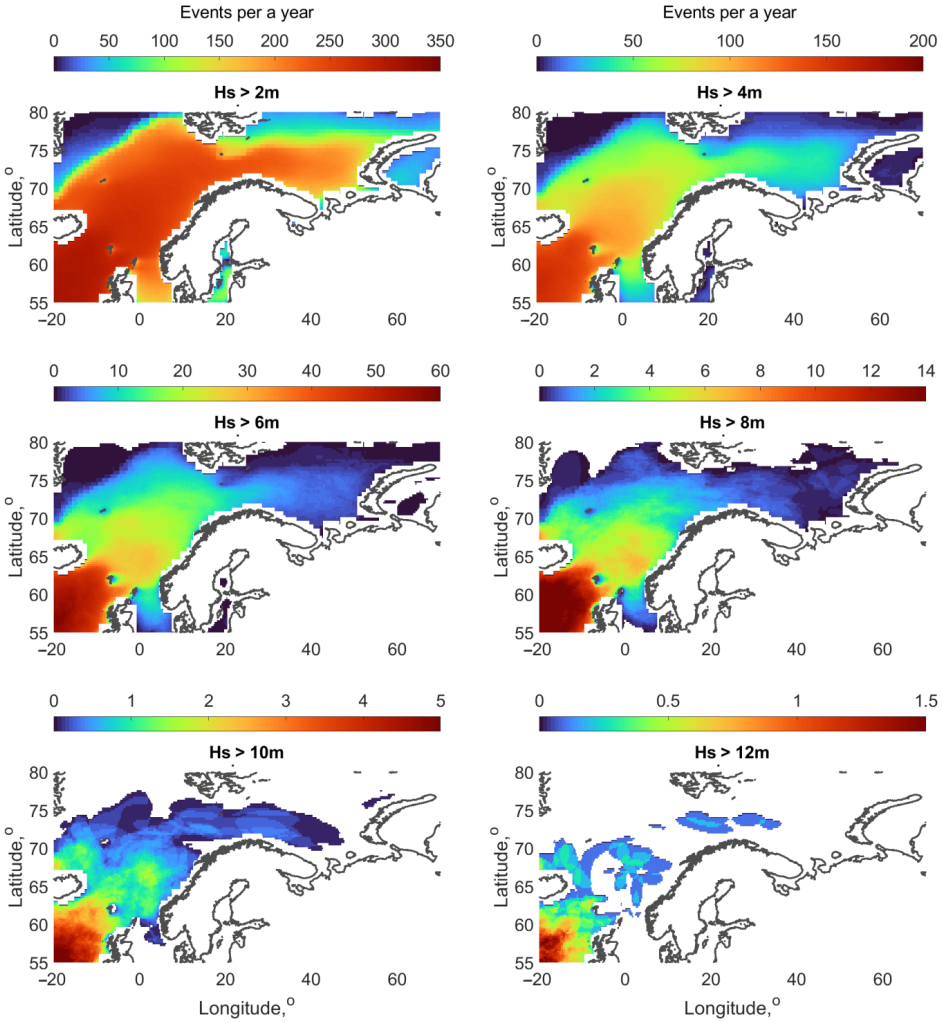

Figure 9. Spatial distribution of the annual number of days when SWHs (either PL-associated, or not) exceed 2 m, 4 m, 6 m, 8 m, 10 m and 12 m from ERA5 data for 2012–2022.

6. Conclusions

The probabilities of abnormally high waves are derived for the regions of the Norwegian, Barents and Eastern Greenland Seas. The analysis builds on PL climatology and the wave model based on the self-similar extended duration laws of wave growth in conditions of short-living moving cyclones. The obtained results are important to better understand the impact of PLs on sea conditions and to also help reduce risks for high-latitude maritime activities, transportation, gas and oil platforms and possible resulting pollution.

Spatial distributions of the annual number of events of wave parameters exceeding specified thresholds are presented. As obtained, the frequency of occurrence of waves with a height larger than 4 m is up to 6 events per year, wave heights larger than 6 m appear 3–5 times per year, wave heights larger than 8 m appear 2–3 times in a year, wave heights larger than 10 m occur once in a year, wave heights larger than 12 m occur once in several years, and 15 m SWHs occur less than once in a decade. The wavelengths of PL-generated waves mostly range from 100 to 300 m, and rarely (once in 5–10 years), 400 m.

These values can be treated as the upper estimates of PL-associated waves probabilities due to crude assumptions of the wave generation by axi-symmetrical cyclonic wind fields moving in the same direction with constant propagation velocity and constant maximum wind speed during the whole PL lifetime. As found, high wind atmospheric systems, which

are not classified as PLs, play important (crucial) role in the frequency of emergence of high surface waves. This frequency can be much larger than the frequency of appearance of high waves generated by PLs. Yet, PLs are apparently the dominating mechanism to form the highest waves in the Barents and the north of the Norwegian Seas.

Author Contributions: Conceptualization, V.K. and B.C.; methodology, V.K. and M.Y.; calculations and formal analysis, M.Y.; writing, M.Y., V.K. and B.C.; visualization, M.Y.; supervision, V.K. All authors have read and agreed to the published version of the manuscript.

Funding: The core support for this work was provided by the Russian Science Foundation Grant No. 21-17-00236. The support of the Ministry of Science and Education of the Russian Federation under State Assignment No. FNNN-2021-0004 at MHI RAS (statistics of wind parameters) and State Assignment No. 0736-2020-0005726 at RSHU (approach and methodology) are gratefully acknowledged. The support of the ESA, France OCEAN+EXTREME MAXSS project C.N.4000132954/20/I-NB is also acknowledged.

Data Availability Statement: ERA5 products are available through the Copernicus Climate Data Store (https://cds.climate.copernicus.eu/cdsapp#!/dataset/reanalysis-era5-single-levels?tab=form, accessed on 22 May 2023).

Conflicts of Interest: The authors declare no conflict of interest. The funders had no role in the design of the study; in the collection, analyses, or interpretation of data; in the writing of the manuscript; or in the decision to publish the results.

References

1. Renfrew, I. Polar lows. In *Encyclopedia of Atmospheric Sciences*; Holton, J.R., Ed.; Academic Press: Oxford, UK, 2003; pp. 1761–1768. [CrossRef]
2. Heinemann, G.; Claud, C. "Report of a Workshop on Theoretical and Observational Studies of Polar Lows" of the European Geophysical Society Polar Lows Working Group. *Bull. Am. Meteorol. Soc.* **1997**, *78*, 2643–2658. [CrossRef]
3. Smirnova, J.E.; Golubkin, P.A.; Bobylev, L.P.; Zabolotskikh, E.V.; Chapron, B. Polar low climatology over the Nordic and Barents Seas based on satellite passive microwave data. *Geophys. Res. Lett.* **2015**, *42*, 5603–5609. [CrossRef]
4. Rojo, M.; Claud, C.; Mallet, P.E.; Noer, G.; Carleton, A.M.; Vicomte, M. Polar low tracks over the Nordic Seas: A 14-winter climatic analysis. *Tellus A Dyn. Meteorol. Oceanogr.* **2015**, *67*, 24660. [CrossRef]
5. Gachon, P.; Laprise, R.; Zwack, P.; Saucier, F.J. The effects of interactions between surface forcings in the development of a model-simulated polar low in Hudson Bay. *Tellus A Dyn. Meteorol. Oceanogr.* **2003**, *55*, 61–87. [CrossRef]
6. Diansky, N.; Panasenkova, I.; Fomin, V. Investigation of the Barents Sea Upper Layer Response to the Polar Low in 1975. *Phys. Oceanogr.* **2019**, *26*, 467–483. [CrossRef]
7. Condron, A.; Renfrew, I. The impact of polar mesoscale storms on northeast Atlantic Ocean circulation. *Nat. Geosci.* **2003**, *6*, 34–37. [CrossRef]
8. Stoll, P.J.; Graversen, R.G.; Noer, G.; Hodges, K. An objective global climatology of polar lows based on reanalysis data. *Q. J. R. Meteorol. Soc.* **2018**, *144*, 2099–2117. [CrossRef]
9. Fletcher, J.; Mason, S.; Jakob, C. The Climatology, Meteorology, and Boundary Layer Structure of Marine Cold Air Outbreaks in Both Hemispheres. *J. Clim.* **2016**, *29*, 1999–2014. [CrossRef]
10. Moreno-Ibáñez, M.; Laprise, R.; Gachon, P. Recent advances in polar low research: Current knowledge, challenges and future perspectives. *Tellus A Dyn. Meteorol. Oceanogr.* **2021**, *73*, 1–31. [CrossRef]
11. Yanase, W.; Niino, H.; Ichi, I.; Watanabe, S.; Hodges, K.; Zahn, M.; Spengler, T.; Gurvich, I.A. Climatology of Polar Lows over the Sea of Japan Using the JRA-55 Reanalysis. *J. Clim.* **2016**, *29*, 419–437. [CrossRef]
12. Dee, D.P.; Uppala, S.M.; Simmons, A.J.; Berrisford, P.; Poli, P.; Kobayashi, S.; Andrae, U.; Balmaseda, M.A.; Balsamo, G.; Bauer, P.; et al. The ERA-Interim reanalysis: Configuration and performance of the data assimilation system. *Q. J. R. Meteorol. Soc.* **2011**, *137*, 553–597. [CrossRef]
13. Bromwich, D.H.; Wilson, A.B.; Bai, L.; Liu, Z.; Barlage, M.; Shih, C.F.; Maldonado, S.; Hines, K.M.; Wang, S.H.; Woollen, J.; et al. The Arctic System Reanalysis, Version 2. *Bull. Am. Meteorol. Soc.* **2018**, *99*, 805–828. [CrossRef]
14. Noer, G.; Saetra, O.; Lien, T.; Gusdal, Y. A climatological study of polar lows in the Nordic Seas. *Q. J. R. Meteorol. Soc.* **2011**, *137*, 1762–1772. [CrossRef]
15. Wilhelmsen, K. Climatological study of gale-producing polar lows near Norway. *Tellus A Dyn. Meteorol. Oceanogr.* **1985**, *37*, 451–459. [CrossRef]
16. Laffineur, T.; Claud, C.; Chaboureau, J.P.; Noer, G. Polar Lows over the Nordic Seas: Improved Representation in ERA-Interim Compared to ERA-40 and the Impact on Downscaled Simulations. *Mon. Weather Rev.* **2014**, *142*, 2271–2289. [CrossRef]
17. Zappa, G.; Shaffrey, L.; Hodges, K. Can Polar Lows be Objectively Identified and Tracked in the ECMWF Operational Analysis and the ERA-Interim Reanalysis? *Mon. Weather Rev.* **2014**, *142*, 2596–2608. [CrossRef]

18. Smirnova, J.; Golubkin, P. Comparing Polar Lows in Atmospheric Reanalyses: Arctic System Reanalysis versus ERA-Interim. *Mon. Weather Rev.* **2017**, *145*, 2375–2383. [CrossRef]
19. Michel, C.; Terpstra, A.; Spengler, T. Polar Mesoscale Cyclone Climatology for the Nordic Seas Based on ERA-Interim. *J. Clim.* **2018**, *31*, 2511–2532. [CrossRef]
20. Young, I.R. Parametric Hurricane Wave Prediction Model. *J. Waterw. Port Coast. Ocean Eng.* **1988**, *114*, 637–652. [CrossRef]
21. Bowyer, P.J.; MacAfee, A.W. The Theory of Trapped-Fetch Waves with Tropical Cyclones—An Operational Perspective. *Weather Forecast.* **2005**, *20*, 229–244. [CrossRef]
22. Young, I.R. A Review of Parametric Descriptions of Tropical Cyclone Wind-Wave Generation. *Atmosphere* **2017**, *8*, 194. [CrossRef]
23. Kudryavtsev, V.; Golubkin, P.; Chapron, B. A simplified wave enhancement criterion for moving extreme events. *J. Geophys. Res. Ocean.* **2015**, *120*, 7538–7558. [CrossRef]
24. Kudryavtsev, V.; Yurovskaya, M.; Chapron, B. Self Similarity of Surface Wave Developments Under Tropical Cyclones. *J. Geophys. Res. Oceans* **2021**, *126*, e16916. [CrossRef]
25. Dysthe, K.B.; Harbitz, A. Big waves from polar lows? *Tellus A Dyn. Meteorol. Oceanogr.* **1987**, *39*, 500–508. [CrossRef]
26. Orimolade, A.P.; Furevik, B.R.; Noer, G.; Gudmestad, O.T.; Samelson, R.M. Waves in polar lows. *J. Geophys. Res. Ocean.* **2016**, *121*, 6470–6481. [CrossRef]
27. Kudryavtsev, V.; Cheshm Siyahi, V.; Yurovskaya, M.; Chapron, B. On Surface Waves in Arctic Seas. *Bound.-Layer Meteorol.* **2022**, *187*, 267–294. [CrossRef]
28. Rojo, M.; Claud, C.; Noer, G.; Carleton, A.M. In Situ Measurements of Surface Winds, Waves, and Sea State in Polar Lows Over the North Atlantic. *J. Geophys. Res. Atmos.* **2019**, *124*, 700–718. [CrossRef]
29. Cavaleri, L.; Barbariol, F.; Benetazzo, A.; Bertotti, L.; Bidlot, J.R.; Janssen, P.; Wedi, N. The Draupner wave: A fresh look and the emerging view. *J. Geophys. Res. Ocean.* **2016**, *121*, 6061–6075. [CrossRef]
30. Kudryavtsev, V.; Zabolotskikh, E.; Chapron, B. Abnormal Wind Waves in the Arctic: Probability of Occurrence and Spatial Distribution. *Russ. Meteorol. Hydrol.* **2019**, *44*, 268–275. [CrossRef]
31. Golubkin, P.; Smirnova, J.; Bobylev, L. Satellite-Derived Spatio-Temporal Distribution and Parameters of North Atlantic Polar Lows for 2015–2017. *Atmosphere* **2021**, *12*, 224. [CrossRef]
32. Polverari, F.; Portabella, M.; Lin, W.; Sapp, J.W.; Stoffelen, A.; Jelenak, Z.; Chang, P.S. On High and Extreme Wind Calibration Using ASCAT. *IEEE Trans. Geosci. Remote Sens.* **2022**, *60*, 1–10. [CrossRef]
33. Bourassa, M.A.; Gille, S.T.; Bitz, C.; Carlson, D.; Cerovecki, I.; Clayson, C.A.; Cronin, M.F.; Drennan, W.M.; Fairall, C.W.; Hoffman, R.N.; et al. High-Latitude Ocean and Sea Ice Surface Fluxes: Challenges for Climate Research. *Bull. Am. Meteorol. Soc.* **2013**, *94*, 403–423. [CrossRef]
34. Lin, W.; Portabella, M.; Stoffelen, A.; Vogelzang, J.; Verhoef, A. ASCAT wind quality under high subcell wind variability conditions. *J. Geophys. Res. Ocean.* **2015**, *120*, 5804–5819. [CrossRef]
35. Kitaigorodski, S. Applications of the theory of similarity to the analysis of wind-generated wave motion as a stochastic process. *Bull. Acad. Sci. USSR Geophys. Ser.* **1962**, *1*, 105–117.
36. Babanin, A.V.; Soloviev, Y.P. Field Investigation of Transformation of the Wind Wave Frequency Spectrum with Fetch and the Stage of Development. *J. Phys. Oceanogr.* **1998**, *28*, 563–576. [CrossRef]
37. Badulin, S.I.; Babanin, A.V.; Zakharov, V.E.; Resio, D. Weakly turbulent laws of wind-wave growth. *J. Fluid Mech.* **2007**, *591*, 339–378. [CrossRef]
38. Zakharov, V.E.; Badulin, S.I.; Geogjaev, V.V.; Pushkarev, A.N. Weak-Turbulent Theory of Wind-Driven Sea. *Earth Space Sci.* **2019**, *6*, 540–556. [CrossRef]
39. Dulov, V.; Kudryavtsev, V.; Skiba, E. On fetch- and duration-limited wind wave growth: Data and parametric model. *Ocean Model.* **2020**, *153*, 101676. [CrossRef]
40. Kudryavtsev, V.; Yurovskaya, M.; Chapron, B. 2D Parametric Model for Surface Wave Development Under Varying Wind Field in Space and Time. *J. Geophys. Res. Oceans* **2021**, *126*, e16915. [CrossRef]
41. Yurovskaya, M.; Kudryavtsev, V.; Mironov, A.; Mouche, A.; Collard, F.; Chapron, B. Surface Wave Developments under Tropical Cyclone Goni (2020): Multi-Satellite Observations and Parametric Model Comparisons. *Remote Sens.* **2022**, *14*, 2032. [CrossRef]
42. Yurovskaya, M.; Kudryavtsev, V.; Chapron, B. A self-similar description of the wave fields generated by tropical cyclones. *Ocean Model.* **2023**, *183*, 102184. [CrossRef]
43. Hersbach, H.; Bell, B.; Berrisford, P.; Biavati, G.; Horanyi, A.; Munoz Sabater, J.; Nicolas, J.; Peubey, C.; Radu, R.; Rozum, I.; et al. ERA5 hourly data on single levels from 1940 to present. *Copernic. Clim. Chang. Serv. (C3s) Clim. Data Store CDS* **2023**, *10*. [CrossRef]
44. Holland, G.J. An analytic model of the wind and pressure profiles in hurricanes. *Mon. Weather Rev.* **1980**, *108*, 1212–1218. [CrossRef]
45. Myslenkov, S.; Platonov, V.; Kislov, A.; Silvestrova, K.; Medvedev, I. Thirty-Nine-Year Wave Hindcast, Storm Activity, and Probability Analysis of Storm Waves in the Kara Sea, Russia. *Water* **2021**, *13*, 648. [CrossRef]
46. Merrill, R.T. A Comparison of Large and Small Tropical Cyclones. *Mon. Weather Rev.* **1984**, *112*, 1408–1418. [CrossRef]
47. Kimball, S.K.; Mulekar, M.S. A 15-Year Climatology of North Atlantic Tropical Cyclones. Part I: Size Parameters. *J. Clim.* **2004**, *17*, 3555–3575. [CrossRef]

48. Wu, L.; Tian, W.; Liu, Q.; Cao, J.; Knaff, J.A. Implications of the Observed Relationship between Tropical Cyclone Size and Intensity over the Western North Pacific. *J. Clim.* **2015**, *28*, 9501–9506. [CrossRef]
49. Kim, H.J.; Moon, I.J.; Oh, I. Comparison of Tropical Cyclone Wind Radius Estimates between the KMA, RSMC Tokyo, and JTWC. *Asia-Pac. J. Atmos. Sci.* **2022**, *58*, 563–576. [CrossRef]
50. Romero, R.; Emanuel, K. Climate Change and Hurricane-Like Extratropical Cyclones: Projections for North Atlantic Polar Lows and Medicanes Based on CMIP5 Models. *J. Clim.* **2017**, *30*, 279–299. [CrossRef]
51. Gebhardt, C.; Bidlot, J.R.; Gemmrich, J.; Lehner, S.; Pleskachevsky, A.; Rosenthal, W. Wave observation in the marginal ice zone with the TerraSAR-X satellite. *Ocean Dyn.* **2016**, *66*, 839–852. [CrossRef]
52. Ardhuin, F.; Stopa, J.; Chapron, B.; Collard, F.; Smith, M.; Thomson, J.; Doble, M.; Blomquist, B.; Persson, O.; Collins, C.O.; et al. Measuring ocean waves in sea ice using SAR imagery: A quasi-deterministic approach evaluated with Sentinel-1 and in situ data. *Remote Sens. Environ.* **2017**, *189*, 211–222. [CrossRef]
53. Shen, H.; Perrie, W.; Hu, Y.; He, Y. Remote Sensing of Waves Propagating in the Marginal Ice Zone by SAR. *J. Geophys. Res. Ocean.* **2018**, *123*, 189–200. [CrossRef]
54. Collard, F.; Marié, L.; Nouguier, F.; Kleinherenbrink, M.; Ehlers, F.; Ardhuin, F. Wind-Wave Attenuation in Arctic Sea Ice: A Discussion of Remote Sensing Capabilities. *J. Geophys. Res. Ocean.* **2022**, *127*, e2022JC018654. [CrossRef]